PCCP

Nearside-farside analysis of differential cross sections: The reaction I + HI → IH + I

C. Noli,[a] J. N. L. Connor,*[a] N. Rougeau[b] and C. Kubach[b]

[a] *Department of Chemistry, University of Manchester, Manchester, UK M13 9PL*
[b] *Laboratoire des Collisions Atomiques et Moléculaires (Unité de Recherches Associée au CNRS No. 281), Bâtiment 351, Université Paris-Sud, 91405 Orsay Cedex, France*

Received 9th May 2001, Accepted 25th June 2001
First published as an Advance Article on the web 31st August 2001

We have carried out quantum calculations of differential cross sections for the state selected reaction, $I + HI(v_i, j_i) \rightarrow IH(v_f, j_f) + I$, where v_i, j_i and v_f, j_f are initial and final vibrational and rotational quantum numbers respectively. The extended London–Eyring–Polanyi–Sato potential energy surface A of Manz and Römelt (J. Manz and J. Römelt, *Chem. Phys. Lett.*, 1981, **81**, 179) was employed. The scattering matrix elements were computed by a quantum method which applies a Born–Oppenheimer type separation to the motion of the light and heavy atoms; a centrifugal-sudden approximation was also made. The scattering calculations were performed for three values of the total energy. Eighteen differential cross sections are reported, which display forward, sideward and backward scattering. Structure in the angular distributions is analysed using a semiclassical optical model. In addition, a nearside-farside (NF) decomposition is applied to the Legendre partial wave series representation of the scattering amplitude. The semiclassical optical model supplies a physical interpretation of the backward scattering in terms of simple classical concepts, but fails to interpret the sideward and forward scattering. In contrast, NF theory nearly always provides a physically clear explanation of the forward, sideward and backward scattering.

I. Introduction

The transfer of an H atom between two I atoms is a chemical reaction of fundamental importance because of the extreme difference in the masses of the light and heavy particles. Indeed, there have been many classical, semiclassical and quantum studies of the collinear[1–3] and three dimensional dynamics[4–14] of the I + HI reaction. It was suggested in ref. 15 that transition state resonances in the I + HI reaction could be observed by photodetaching the corresponding anion, IHI^-. This suggestion was confirmed experimentally by Neumark *et al.*[16] as well as in theoretical simulations of the photodetachment spectrum.[5,7,10,12,13,16,17] The IHI system also exhibits two novel dynamical phenomena. The first is the 'smooth step effect'[5,18] in the energy dependence of integral cross sections;[9,11,12] the step is centred at the resonance energy for the partial wave with zero total angular momentum quantum number. The second is the occurrence of 'vibrational bonding', whereby the three–dimensional IHI molecule possesses a bound state on a minimum-free potential energy surface.[3,6–9,12,15,19]

One property that has received little attention to date is the differential cross section for reactive scattering. It contains important information on the detailed dynamics of the H atom transfer.[9] The purpose of our paper is to rectify this deficiency. We make three contributions to understanding the angular scattering of the state selected reaction

$$I + HI(v_i, j_i) \rightarrow IH(v_f, j_f) + I$$

where v_i, j_i and v_f, j_f are vibrational and rotational quantum numbers for the initial and final states respectively:

1. We report eighteen differential cross sections calculated by the (approximate) quantum method of Richard-Viard *et al.*[9] This method applies a Born–Oppenheimer type separation to the dynamics of the I + HI reaction. Our angular distributions extend earlier results in Fig. 4 and 5 of ref. 9. In our calculations, the Legendre partial wave series representation of the scattering amplitude contains up to 150 numerically significant terms, which makes it difficult (or impossible) to understand the physical origin of structure in the quantum differential cross sections.

2. We compare the quantum angular distributions obtained in contribution (1) with the results from a semiclassical optical model,[20] which is a simple procedure for calculating the differential cross sections of chemical reactions. The semiclassical optical model lets us understand some features of the quantum angular scattering in terms of simple classical concepts.

3. We report nearside–farside (NF) analyses of the quantum angular distributions. The NF technique[21–33] is a straightforward procedure for understanding structure in differential cross sections. It decomposes the scattering amplitude into two subamplitudes (one N, the other F). Structure in an angular distribution can arise from the N subamplitude, or from the F subamplitude, or from interference between the N and F subamplitudes. A NF analysis has the advantage that semiclassical techniques such as saddle point or stationary phase integration are not used, although the semiclassical picture is still evident.[21–33]

Section II describes the quantum calculation of the scattering matrix elements for I + HI and the corresponding angular distributions. Our results from the semiclassical optical model are presented in section III. NF theory and its application to I + HI are the subjects of section IV. Our conclusions are in section V.

II. Quantum calculation of reactive angular scattering

This section describes the potential energy surface for I + HI, the quantum method used to calculate the scattering matrix

 DOI: 10.1039/b104099p

elements, the partial wave series for the reactive differential cross sections, and the resulting angular distributions.

A. Potential energy surface

We used the isoergic London–Eyring–Polanyi–Sato (LEPS) potential surface A introduced by Manz and Römelt.[1] This LEPS surface has a symmetric saddle point located at an I–H distance of $r_{IH}^{\ddagger} = 1.794$ Å, with a classical barrier height of 48 meV. The saddle point occurs for the collinear configuration of I–H–I. By analogy with the Cl–H–Cl system,[34,35] it is likely that the true IHI surface has a non-collinear saddle point. However, there is no accurate *ab initio* surface for IHI at the present time.

B. Quantum calculation of the scattering matrix

The scattering matrix elements were calculated by the method of Richard-Viard *et al.*[9] (see also ref. 36 for related work). This method applies a Born–Oppenheimer type separation to the dynamics of a heavy + light–heavy atom reaction.[6–12] The motion of the three atoms is treated in two steps:[9]

1. The Schrödinger equation for the motion of the H atom is first solved for fixed values of the I–I distance. The corresponding eigenfunctions are adiabatic wavefunctions for the H atom and the eigenvalues are adiabatic potential curves. In practice, it is more convenient to use nearly diabatic states whose construction is now outlined.

The hydrogenic wavefunctions are taken as linear combinations of functions that describe H when it is attached to each I atom (by analogy with the linear-combination-of-atomic-orbitals method for electronic wavefunctions). The basis set consists of rovibrational functions, centred on each I, which are products of a Morse wavefunction for the vibrational motion and a spherical harmonic for the rotational motion. More precisely, 25 and 15 rotor states for the isolated molecules IH($v = 0$) and IH($v = 1$) respectively were used with Morse parameters, $r_e = 1.609$ Å, $\omega_e = 2300.5$ cm^{-1} and $\omega_e x_e = 53.0$ cm^{-1}. In addition, we added to the basis set 16 rotor states for each vibrational state of the 'pseudo-molecule' IH($v = 0,1$) with Morse parameters, $r_e = R_{II}/2$, $\omega_e = 1300.0$ cm^{-1} and $\omega_e x_e = 53.0$ cm^{-1}, where R_{II} is the I–I distance. Adding the pseudo-molecule wavefunctions to the basis provides flexibility in describing the motion of the H atom when it is between the two I atoms (otherwise a huge basis set of isolated IH wavefunctions would be required).[9]

Next, these basis functions are linearly combined to produce hydrogenic wavefunctions of σ_g or σ_u symmetry (states with $\pi_{g,u}$, $\delta_{g,u}$, ... symmetries are neglected). Then, for each symmetry, orthonormal wavefunctions are constructed using the Schmidt orthogonalization procedure. The orthogonalization has been performed in the following order: first the 25 $v = 0$ functions (from $j = 0$ to $j = 24$), then the 15 $v = 1$ functions (from $j = 0$ to $j = 14$), then the 16 $v = 0$ functions of the pseudo-molecule (from $j = 0$ to $j = 15$) and finally the 16 $v = 1$ functions of the pseudo-molecule (from $j = 0$ to $j = 15$). This procedure produces wavefunctions having a weak R_{II} dependence and constitutes a nearly diabatic representation for the H atom motion.

The symmetrized and orthonormalized basis set described above is unnecessarily large for the calculation of the scattering matrix at the low total energies (<30 meV) of interest in this paper, where only the IH($v = 0$, $j \leqslant 5$) channels are open. We thus limited the nearly diabatic basis to the lowest 20 states, which correlate asymptotically to IH($v = 0$, $j = 0$–19) + I. However in σ_g symmetry, this basis set does not accurately reproduce the potential energy well responsible for the two lowest resonances in the I + HI dynamics.[9] We therefore added in g symmetry the 'efficient $v = 1$ state', and the three lowest 'adiabatic pseudostates' (see ref. 9 for additional information).

2. In the second step, the total wavefunction for the I + HI reaction is expanded in terms of the nearly diabatic states constructed in step (1). The coefficients in this expansion describe the motion of the two I atoms, and are further expanded in a Legendre partial wave series. The coefficients of the partial wave series satisfy a set of coupled ordinary differential equations. We make a centrifugal sudden approximation which retains only states with $\Omega = 0$, where Ω is the projection quantum number for the total angular momentum quantum number, J, on the I–I axis (this is the same approximation as retaining only σ_g and σ_u hydrogenic states in the nearly diabatic basis).[9] The solutions of the coupled equations for g and u symmetry yield the corresponding scattering (S) matrices $\boldsymbol{S}_g^J$ and $\boldsymbol{S}_u^J$ respectively, from which the $\boldsymbol{S}^J$ matrix for the reaction can be constructed using[9]

$$\boldsymbol{S}^J = \tfrac{1}{2}(\boldsymbol{S}_g^J - \boldsymbol{S}_u^J), \quad J = 0, 1, 2, \ldots$$

More details on the calculation of the S matrix can be found in ref. 6–9.

C. Quantum calculation of the differential cross section

The scattering amplitude for the reaction is given by the Legendre partial wave series (PWS)[9]

$$f_{v_f j_f \leftarrow v_i j_i}(\theta_R) = \frac{1}{2ik_{v_i j_i}} \sum_{J=0}^{\infty} (2J+1) S^J_{v_f j_f \leftarrow v_i j_i} P_J(\cos\theta_R) \quad (2.1)$$

where $k_{v_i j_i}$ is the initial translational wavenumber, $P_J(\bullet)$ is a Legendre polynomial of degree J and θ_R is the reactive scattering angle, *i.e.*, the angle between the direction of the outgoing IH molecule and the incoming I atom [*n.b.*, in ref. 9, θ_R

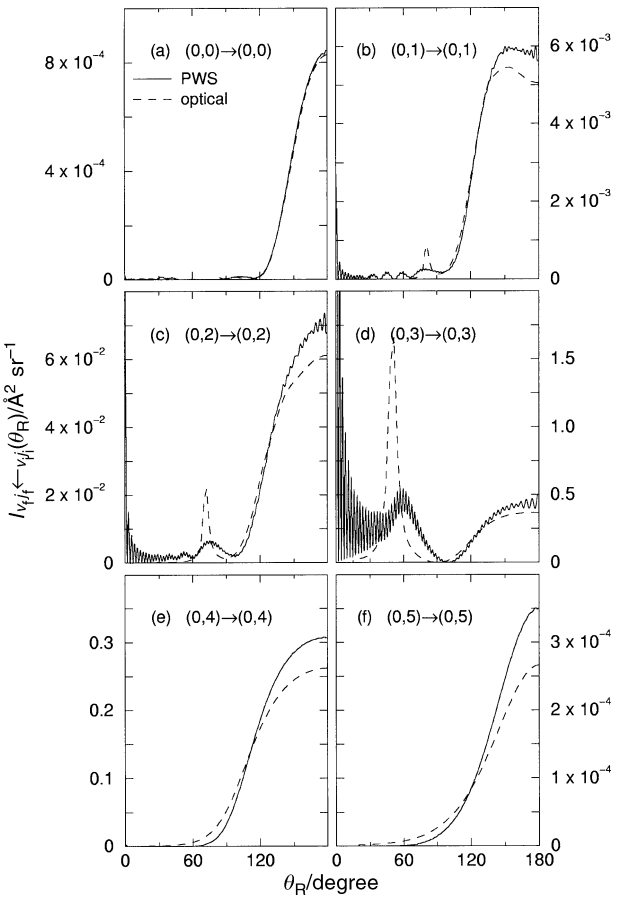

Fig. 1 Plot of the angular distribution, $I_{v_f j_f \leftarrow v_i j_i}(\theta_R)$, *vs.* reactive scattering angle, θ_R, for the I + HI(v_i, j_i) → IH(v_f, j_f) + I reaction at $E = 29.5$ meV. Solid line: PWS angular distribution. Dashed line: Semiclassical optical model angular distribution. The transitions shown are, (a) (0,0) → (0,0), (b) (0,1) → (0,1), (c) (0,2) → (0,2), (d) (0,3) → (0,3), (e) (0,4) → (0,4), (f) (0,5) → (0,5).

is denoted θ, and in ref. 23, $\boldsymbol{S}^J$ is denoted $\tilde{\boldsymbol{S}}^J$].The state-to-state differential cross section is given by

$$I_{v_f j_f \leftarrow v_i j_i}(\theta_R) = |f_{v_f j_f \leftarrow v_i j_i}(\theta_R)|^2 \qquad (2.2)$$

We will use the abbreviation 'PWS' for cross sections computed from eqn. (2.1) and (2.2). We carried out calculations at three values of the total energy E, namely 29.5, 26.8 and 21.3 meV, where $E = 0$ meV corresponds to the zero point energy of the isolated IH($v_i = 0$, $j_i = 0$) molecule. Since the LEPS surface is asymptotically Morse for I + HI, the rovibrational energies of IH(v_i,j_i) were calculated using the analytic formula for the vibrational energy levels of a Morse oscillator, plus the rigid rotor approximation for the rotational motion with an equilibrium distance of $r_e = 1.609$ Å. The masses used in the calculations are $m_H = 1.008$ u and $m_I = 126.9$ u. At $E = 21.3$ meV, the channels $v_i = 0$, $j_i \leqslant 4$ are open, whereas at $E = 26.8$ meV and $E = 29.5$ meV, the channel $v_i = 0$, $j_i = 5$ is also open. Up to 150 partial waves were required to converge the PWS at the three energies.

D. Results

Here we report our results for the PWS angular distributions calculated from eqn. (2.1) and (2.2). We do not show differential cross sections for all possible transitions at the three values of E (57 independent cross sections in all); rather we have selected 18 angular distributions that illustrate the various trends and which possess interesting features.

Fig. 1–3 display our PWS results for six transitions at $E = 29.5$, 26.8, 21.3 meV respectively (the dashed lines in these figures will be discussed in section III). Fig. 1 shows, for $E = 29.5$ meV, the angular distributions for the diagonal transitions $(0,j_i) \rightarrow (0,j_f = j_i)$ with $j_i = 0$, 1, 2, 3, 4, 5, where we will

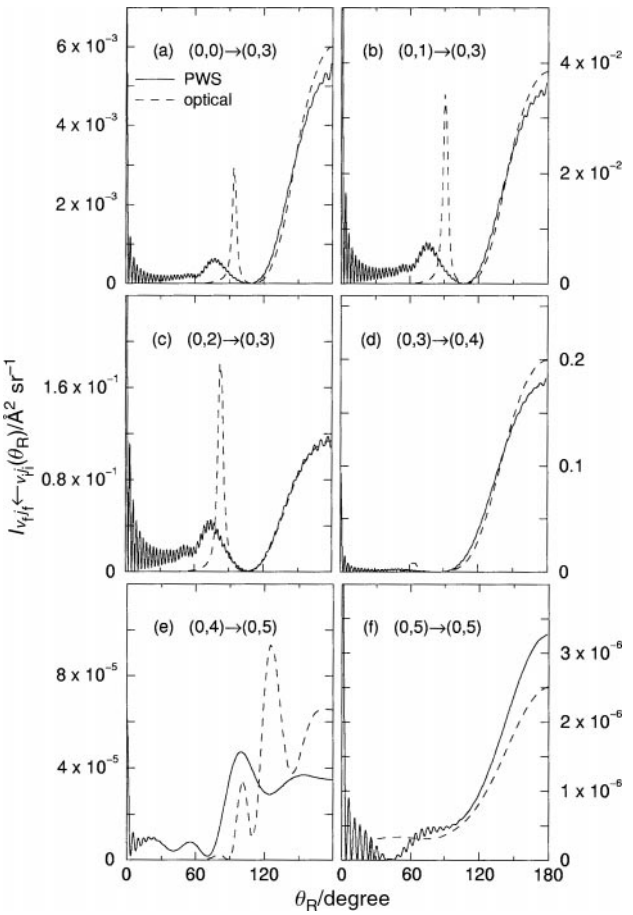

Fig. 2 Same as Fig. 1 except for $E = 26.8$ meV and the transitions (a) (0,0) → (0,3), (b) (0,1) → (0,3), (c) (0,2) → (0,3), (d) (0,3) → (0,4), (e) (0,4) → (0,5), (f) (0,5) → (0,5).

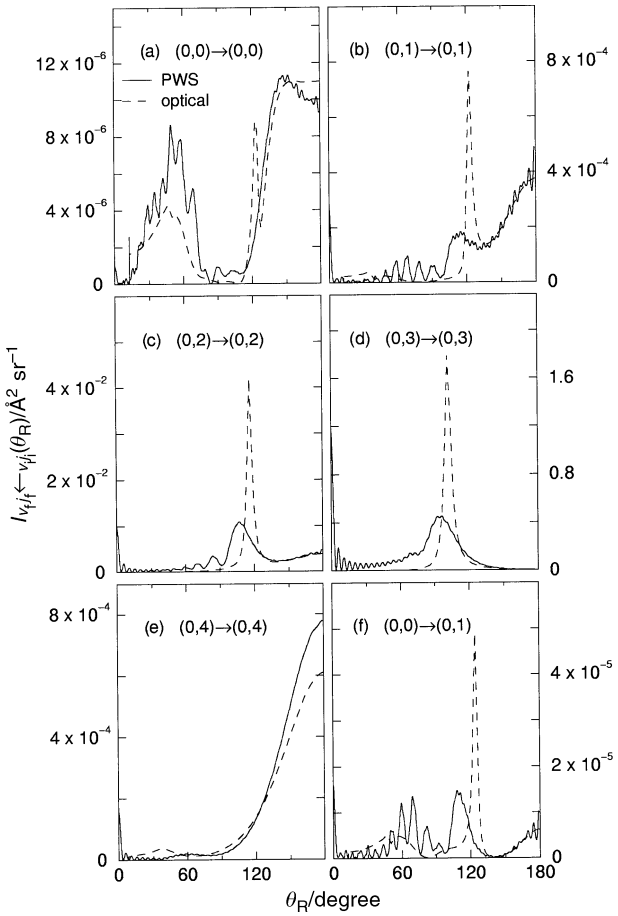

Fig. 3 Same as Fig. 1 except for $E = 21.3$ meV and the transitions (a) (0,0) → (0,0), (b) (0,1) → (0,1), (c) (0,2) → (0,2), (d) (0,3) → (0,3), (e) (0,4) → (0,4), (f) (0,0) → (0,1).

label the transitions $(v_i,j_i) \rightarrow (v_f,j_f)$ from now on. The scattering is mainly in the backward direction, except for the (0,3) → (0,3) transition where forward scattering predominates. The results displayed in Fig. 2 at $E = 26.8$ meV for the transitions (0,0) → (0,3), (0,1) → (0,3), (0,2) → (0,3), (0,3) → (0,4), (0,4) → (0,5) and (0,5) → (0,5), show forward, sideward and backward scattering and are more structured than the cross sections in Fig. 1. The same is also true for the angular scattering in Fig. 3 at $E = 21.3$ meV for the $(0,j_i) \rightarrow (0,j_i)$, $j_i = 0$, 1, 2, 3, 4 and (0,0) → (0,1) transitions.

We make the following general observations on our results in Fig. 1–3:

1. Fig. 4 of ref. 9 shows differential cross sections for the (0,3) → (0,3) transition at $E = 18.6$, 21.3, 24 and 29.5 meV. Our angular distribution at $E = 21.3$ meV in Fig. 3(d) agrees well with the corresponding result in ref. 9. However, there are differences at $E = 29.5$ meV [our Fig. 1(d)] and the plot in ref. 9 was mislabelled, being for a different value of E.

2. The largest cross section at all three values of E is that for the (0,3) → (0,3) transition. This observation has been explained in ref. 7 and 9, using a two state model.

3. There is an expected shift from forward to backward scattering as E decreases.

It is evident that explaining the structure in the angular distributions of Fig. 1–3 will not be a simple matter. In the next section, we describe and discuss the differential cross sections obtained from the semiclassical optical model.

III. Semiclassical optical model

A. Introduction

The semiclassical optical model, introduced by Herschbach,[20] is a straightforward procedure for calculating the angular dis-

tributions of chemical reactions. It has subsequently been applied to a number of reactions,[5,23,31,35,37] which have demonstrated that the model has the following advantages:

No knowledge of the phase of each S matrix element is required. Rather the optical model uses the quantum reaction probability, which is defined by

$$P^J_{v_f j_f \leftarrow v_i j_i} = |S^J_{v_f j_f \leftarrow v_i j_i}|^2, \quad J = 0, 1, 2, \ldots \tag{3.1}$$

The equations expressing the optical model differential cross section in terms of $P^J_{v_f j_f \leftarrow v_i j_i}$ are simple. (See section III.B.)

Close agreement between the optical and PWS angular distributions implies that the quantum angular scattering can be understood using simple classical concepts. Indeed, the optical model can be classified as an approximate nearside theory. It is also a limiting case of the complex angular momentum theory of reactive scattering developed in ref. 22 and 23.

Conversely, a disagreement between the optical and PWS angular distributions implies the need for a more elaborate theoretical analysis of the quantum angular scattering.

B. Theory

The semiclassical optical model makes three main assumptions:[5,20,23,31]

1. Since the two I atoms are much heavier than the H atom, their motion is assumed to be unperturbed by the presence of H. It is also assumed that the I atoms can be represented by hard spheres of radius r, for which the differential cross section is isotropic, being given by

$$I^{hs}(\theta_R) = r^2$$

This result implies direct reaction dynamics, with a one-to-one correspondence between the impact parameter b and θ_R, given by the hard sphere result

$$b = 2r \cos(\theta_R/2) \tag{3.2}$$

for $b \leqslant 2r$. When $b > 2r$ we have $\theta_R = 0$.

2. The role of the transferred H atom is to determine which impact parameters lead to reaction. Denoting the E-dependent reaction probability distribution function by $P_{v_f j_f \leftarrow v_i j_i}(b)$, the angular distribution for the optical model is given by

$$I^{opt}_{v_f j_f \leftarrow v_i j_i}(\theta_R) = r^2 P_{v_f j_f \leftarrow v_i j_i}(b(\theta_R)), \quad b \leqslant 2r$$
$$= 0, \quad b > 2r$$

and eqn. (3.2) is also used.

3. We must also relate $P_{v_f j_f \leftarrow v_i j_i}(b)$ to the E-dependent quantum reaction probability $P^J_{v_f j_f \leftarrow v_i j_i}$. To do this we assume that

$$b \approx J/k_{v_i j_i}$$

This approximation, which neglects the difference between orbital and total angular momentum, should be valid for heavy + light–heavy atom reactions with $j_i \leqslant 5$.

We then have

$$P_{v_f j_f \leftarrow v_i j_i}(b) \approx P^J_{v_f j_f \leftarrow v_i j_i}$$

and

$$I^{opt}_{v_f j_f \leftarrow v_i j_i}(\theta_R) = r^2 P^J_{v_f j_f \leftarrow v_i j_i} \tag{3.3}$$

where

$$J = 2rk_{v_i j_i} \cos(\theta_R/2) \tag{3.4}$$

Eqn. (3.3) and (3.4) are valid for $J \leqslant 2rk_{v_i j_i}$. When $J > 2rk_{v_i j_i}$, we have $I^{opt}_{v_f j_f \leftarrow v_i j_i}(\theta_R) \equiv 0$. In practice, it is easier to compute the angular distributions on a grid of θ_R values using

$$\theta_R = 2 \cos^{-1}(J/(2rk_{v_i j_i})) \quad \text{for } J = 0, 1, 2, \ldots \leqslant 2rk_{v_i j_i}$$

C. Results

The assumptions of the semiclassical optical model imply that, in practice, the model should work best for rebound reactions. These give rise to mainly backward scattering, which results from a repulsive interaction between the reactants.

The only adjustable parameter in the optical model is r. We optimized r by fitting $I^{opt}_{v_f j_f \leftarrow v_i j_i}(\theta_R)$ to the PWS cross section for the (0,0) → (0,0) transition at $E = 29.5$ meV, for which backward scattering is dominant. Fig. 1(a) shows excellent agreement betweeen the two angular distributions. The resulting value of r is 1.56 Å, which was subsequently used for all transitions at the three values of E. Note that $r = 1.56$ Å $< r^{\ddagger}_{IH} = 1.794$ Å, which is consistent with the backward scattering arising from small impact parameter collisions, rather than being determined by the geometry of the collinear saddle point. It is also interesting to compare $2r$ with Fig. 1 of ref. 9, which shows a plot of 'quasi-diabatic' hydrogenic potential energy curves *vs.* R_{IH}. The value $2r = 3.12$ Å lies, as expected, inside the classically forbidden region of the hydrogenic potential curves.

Fig. 1–3 show that the optical model is generally successful in reproducing the scattering into backward angles, although the relative error is often larger for the smaller cross sections. At sideward angles, the peak in the optical model result is usually much larger (factor of 2 or 3) than the corresponding nearby PWS peak. At forward angles, the optical model fails to reproduce the PWS scattering and, in particular, the high frequency oscillations.

In order to understand better the PWS and optical model angular distributions in Fig. 1–3, we show in Fig. 4–6 the corresponding quantum reaction probabilities (3.1) plotted

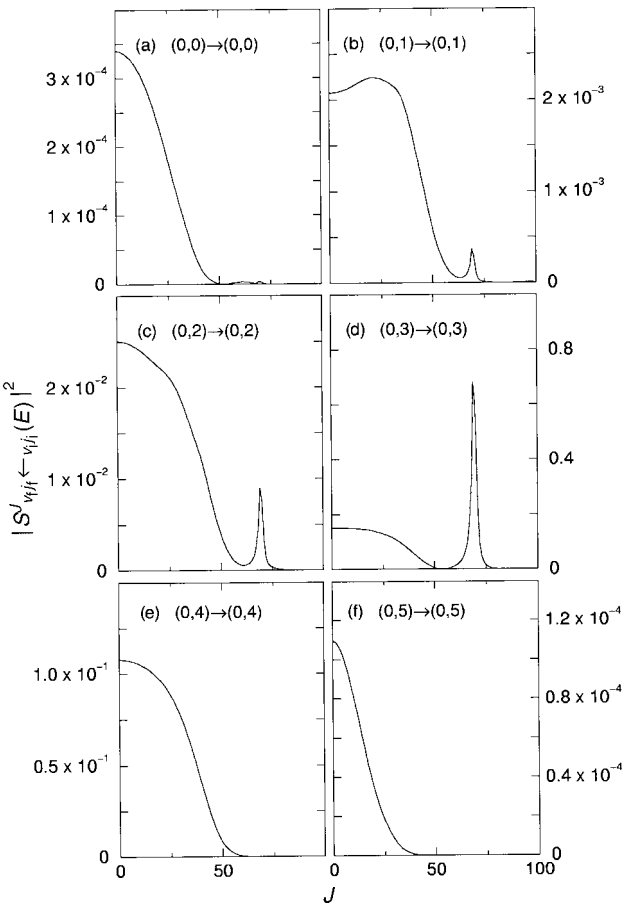

Fig. 4 Plot of the quantum reaction probability, $P^J_{v_f j_f \leftarrow v_i j_i} \equiv |S^J_{v_f j_f \leftarrow v_i j_i}|^2$, *vs.* total angular momentum quantum number, J, for the $I + HI(v_i, j_i) \rightarrow IH(v_f, j_f) + I$ reaction at $E = 29.5$ meV, for the transitions (a) (0,0) → (0,0), (b) (0,1) → (0,1), (c) (0,2) → (0,2), (d) (0,3) → (0,3), (e) (0,4) → (0,4), (f) (0,5) → (0,5).

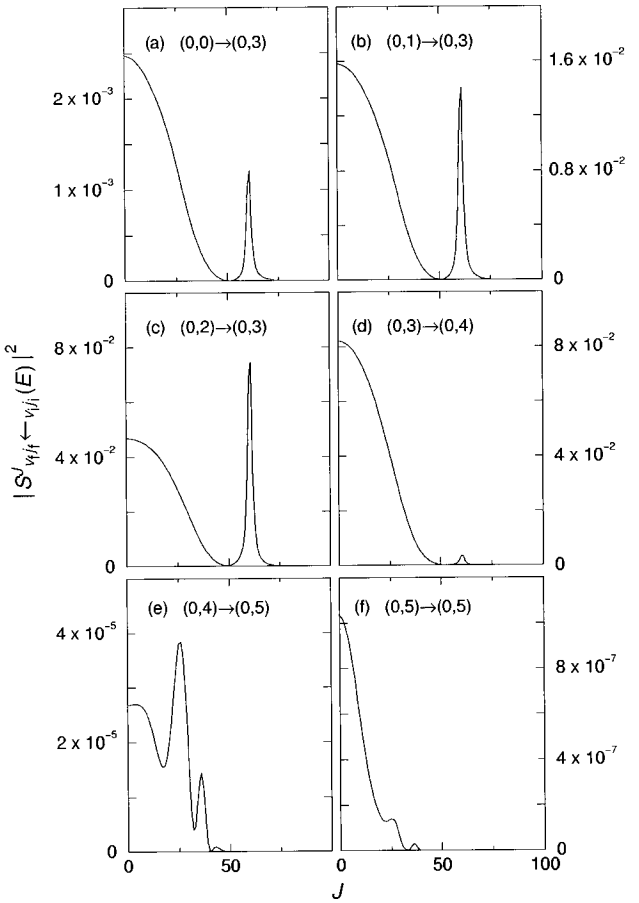

Fig. 5 Same as Fig. 4 except for $E = 26.8$ meV and the transitions (a) (0,0) → (0,3), (b) (0,1) → (0,3), (c) (0,2) → (0,3), (d) (0,3) → (0,4), (e) (0,4) → (0,5), (f)(0,5) → (0,5).

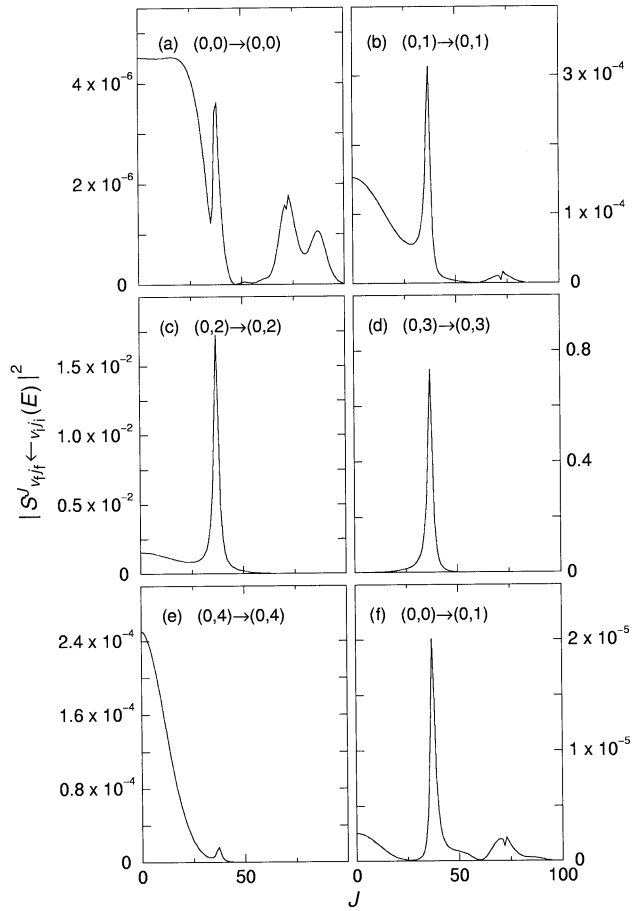

Fig. 6 Same as Fig. 4 except for $E = 21.3$ meV and the transitions (a) (0,0) → (0,0), (b) (0,1) → (0,1), (c) (0,2) → (0,2), (d) (0,3) → (0,3), (e) (0,4) → (0,4), (f) (0,0) → (0,1).

against J. Particularly noticeable in the plots are the resonance peaks for some transitions which occur at $J = 69$, 61, 37 for $E = 29.5$, 26.8, 21.3 meV respectively. This is an example of the J-shift effect,[38] *i.e.*, a decrease in E corresponds to a decrease in the rotational energy of the I–H–I complex. A least squares fit of this resonance (J, E_J) data to the rigid rotator expression

$$E_J = E_0 + BJ(J + 1) \tag{3.5}$$

yields $E_0 = 17.9$ meV and $B = 2.38 \times 10^{-3}$ meV. The value for E_0 is consistent with Fig. 3 of ref. 9, which shows a resonance close to 17.9 meV in a plot of the $J = 0$ reaction probability for $v_i = 0$, $j_i = 3$ (and summed over all final states) *vs.* E.

We can also estimate the bond length of the I–H–I complex from the rotor constant using $B = \hbar^2/2I$ where $I = 2m_H r_{IH}^2$ is the moment of inertia of the collinear symmetric I–H–I complex about a perpendicular axis passing through its centre of mass (r_{IH} is the I–H distance). We obtain the value $r_{IH} = 1.86$ Å, which is somewhat larger than $r_{IH}^{\ddagger} = 1.794$ Å. Note that $2r_{IH} = 3.72$ Å is only slightly larger than the position of the minimum, $R_{II} = 3.62$ Å, of the quasi-diabatic σ_g hydrogenic potential curve responsible for the lowest resonances (see Fig. 1 of ref. 9). This is the expected result for a calculation which assumes a mean value of r_{IH}.

In Fig. 6(a), (b), (f) for $E = 21.3$ meV, there are small blips visible near $J = 73$. These are not numerical artefacts; rather they are the signature of a narrow resonance whose location J-shifts down[9] to $E \approx 8$ meV for $J = 0$. According to eqn. (3.5), the blips are expected to occur at $J = 87$ and $J = 93$ for $E = 26.8$ meV and $E = 29.5$ meV respectively. However, the blips are not visible in Fig. 4 and 5 because of the linear scales along the ordinates of the graphs.

We now discuss the optical model results of Fig. 1-3 in more detail. As required by eqn. (3.3) and (3.4), the angular scattering for the optical model is a distorted mirror image of the corresponding plot of $P^J_{v_f j_f \leftarrow v_i j_i}$ *vs.* J. In particular the resonance peaks, which are determined by eqn. (3.3) and (3.4), are clearly visible in $I^{opt}_{v_f j_f \leftarrow v_i j_i}(\theta_R)$; they arise because the optical model assumes direct specular collision dynamics. As noted above, these pronounced resonance peaks are not present in the PWS angular scattering; rather the corresponding PWS peaks are lower in intensity and broader as well as being slightly displaced. This behaviour can be understood because a resonance implies that a relatively long-lived IHI complex is formed. Rotation and decay of the complex will give rise to an exponential tail stretching into the forward direction. Note that the value $r = 1.56$ Å corresponds to $J_{max} = 2rk_{00} = 94$ at $E = 29.5$ meV, which, as Fig. 4(a) shows, includes all significant partial waves. The same is true for the other transitions in Fig. 4–6.

The analysis of the angular scattering presented above using the semiclassical optical model could be improved in two ways:

A different optimized value of r could be used for each transition and E. This would improve the agreement with the corresponding PWS cross sections at backward angles. However no systematic improvement at sideward and forward angles would be obtained. We have confirmed this behaviour by using $r = r_{IH}^{\ddagger} = 1.794$ Å in eqn. (3.3) and (3.4).

The optical model could be generalized to a 'sticky optical model'.[23] This would take into account the rotation and decay of the IHI complex into the forward direction. However the high frequency oscillations at forward angles would still not be reproduced because of the classical nature of the sticky optical model.[23]

Rather than improve the optical model along these lines, we consider instead in the next section, a NF analysis of the PWS differential cross sections.

IV. Nearside-farside analysis

This section summarizes NF theory for a Legendre PWS[24] and presents our results for the I + HI reaction.

A. Theory

In a NF analysis,[21–33] the PWS scattering amplitude (2.1) is exactly partitioned into the sum of two subamplitudes, N and F, which correspond to angular partial waves travelling clockwise and anticlockwise in θ_R respectively. We write[24]

$$f_{v_f j_f \leftarrow v_i j_i}(\theta_R) = f^{(+)}_{v_f j_f \leftarrow v_i j_i}(\theta_R) + f^{(-)}_{v_f j_f \leftarrow v_i j_i}(\theta_R) \quad (4.1)$$

where

$$f^{(\pm)}_{v_f j_f \leftarrow v_i j_i}(\theta_R) = \frac{1}{2ik_{v_i j_i}} \sum_{J=0}^{\infty} (2J+1) S^J_{v_f j_f \leftarrow v_i j_i} Q^{(\pm)}_J(\cos\theta_R) \quad (4.2)$$

In eqn. (4.2), the $Q^{(\pm)}_J(\cos\theta_R)$ are travelling Legendre functions of degree J, which are obtained by exactly decomposing the Legendre polynomials in eqn. (2.1) according to

$$P_J(\cos\theta_R) = Q^{(+)}_J(\cos\theta_R) + Q^{(-)}_J(\cos\theta_R), \quad J = 0, 1, 2, \ldots, \quad (4.3)$$

We use the Fuller decomposition[39] in eqn. (4.3), where the explicit formulae for the $Q^{(\pm)}_J(\cos\theta_R)$ are given by (for $\theta_R \neq 0, \pi$)

$$Q^{(\pm)}_J(\cos\theta_R) = \frac{1}{2}\left[P_J(\cos\theta_R) \mp \frac{2i}{\pi} Q_J(\cos\theta_R)\right], \quad J = 0, 1, 2, \ldots, \quad (4.4)$$

In eqn. (4.4), $Q_J(\cos\theta_R)$ is a Legendre function of the second kind of degree J. For $J \sin\theta_R \gg 1$, the following asymptotic formulae are valid[24]

$$P_J(\cos\theta_R) \sim \left[\frac{2}{\pi(J+\frac{1}{2})\sin\theta_R}\right]^{1/2} \cos\left[\left(J+\frac{1}{2}\right)\theta_R - \frac{1}{4}\pi\right]$$

and

$$Q_J(\cos\theta_R) \sim -\left[\frac{\pi}{2(J+\frac{1}{2})\sin\theta_R}\right]^{1/2} \sin\left[\left(J+\frac{1}{2}\right)\theta_R - \frac{1}{4}\pi\right]$$

We then obtain from eqn. (4.4)

$$Q^{(\pm)}_J(\cos\theta_R) \sim \left[\frac{1}{2\pi(J+\frac{1}{2})\sin\theta_R}\right]^{1/2} \times \exp\left[\pm i\left[\left(J+\frac{1}{2}\right)\theta_R - \frac{1}{4}\pi\right]\right] \quad (4.5)$$

which is also valid for $J \sin\theta_R \gg 1$

We next identify $Q^{(+)}_J(\cos\theta_R)$ with a F angular wave and $Q^{(-)}_J(\cos\theta_R)$ with a N angular wave. We can do this because the term $\exp[+i(J+\frac{1}{2})\theta_R]$ in eqn. (4.5) physically represents a travelling angular wave moving anticlockwise in θ_R and a semiclassical analysis shows that it typically originates from the farside of the target for an observer in the upper half of the scattering plane at infinity.[24] Similarly, we can identify $Q^{(-)}_J(\cos\theta_R)$ with a N angular wave. Then $f^{(-)}_{v_f j_f \leftarrow v_i j_i}(\theta_R)$ represents the N angular scattering and $f^{(+)}_{v_f j_f \leftarrow v_i j_i}(\theta_R)$ represents the F angular scattering. The corresponding F and N cross sections are

$$I^{(\pm)}_{v_f j_f \leftarrow v_i j_i}(\theta_R) = |f^{(\pm)}_{v_f j_f \leftarrow v_i j_i}(\theta_R)|^2 \quad (4.6)$$

and we also have from eqn. (2.2) and (4.1) the identity

$$I_{v_f j_f \leftarrow v_i j_i}(\theta_R) = |f^{(+)}_{v_f j_f \leftarrow v_i j_i}(\theta_R) + f^{(-)}_{v_f j_f \leftarrow v_i j_i}(\theta_R)|^2 \quad (4.7)$$

Eqn. (4.7) shows that structure in the full PWS differential cross section can arise from the N subamplitude or from the F subamplitude or from interference between the N and the F subamplitudes.

B. Results

Our NF and PWS angular distributions are shown in Fig. 7–9 for the same transitions and E values already used in Fig. 1–3 respectively. In order to display the F cross sections clearly, as well as the forward angle scattering for all three cross sections, $\log I_{v_f j_f \leftarrow v_i j_i}(\theta_R)$ is plotted in Fig. 7–9 rather than $I_{v_f j_f \leftarrow v_i j_i}(\theta_R)$.

Examination of Fig. 7–9 reveals the following trends: $I^{(-)}_{v_f j_f \leftarrow v_i j_i}(\theta_R)$ and $I^{(+)}_{v_f j_f \leftarrow v_i j_i}(\theta_R)$ usually contain less or comparable structure than does $I_{v_f j_f \leftarrow v_i j_i}(\theta_R)$. In addition, the magnitudes of the N and F cross sections are usually similar or smaller than the magnitude of the corresponding full PWS cross section. This means the NF decomposition of eqn. (4.1)–(4.4) *is* providing us with useful results in the sense of being physically meaningful (*n.b.*, there is no guarantee that useful results will in fact be obtained because the NF decomposition of eqn. (4.1)–(4.4) is *not* unique).[24,29,30] An apparent exception is the F cross section which sometimes possesses more structure than does $I_{v_f j_f \leftarrow v_i j_i}(\theta_R)$ or $I^{(-)}_{v_f j_f \leftarrow v_i j_i}(\theta_R)$. However this behav-

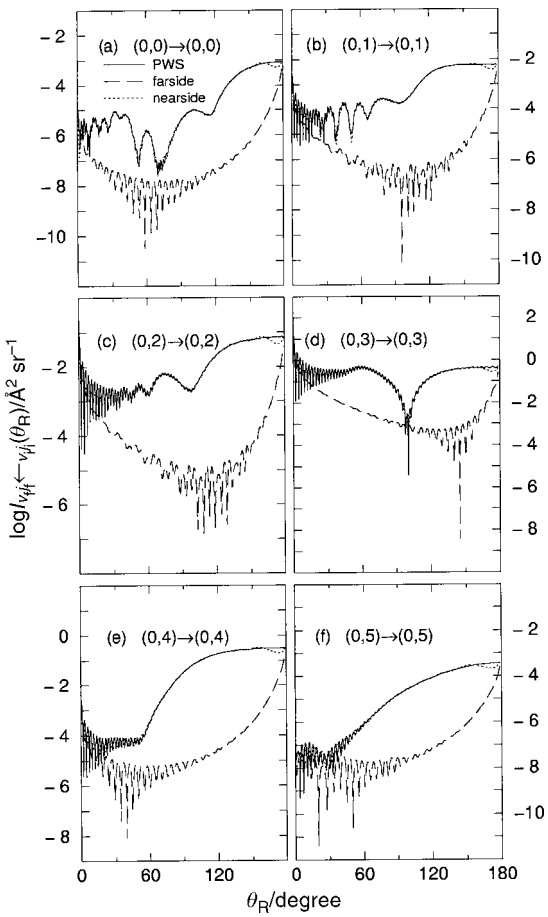

Fig. 7 Plot of the logarithm of the angular distribution, $\log I_{v_f j_f \leftarrow v_i j_i}(\theta_R)$, *vs.* reactive scattering angle, θ_R, for the I + HI(v_i, j_i) → IH(v_f, j_f) + I reaction at E = 29.5 meV. Solid line: PWS angular distribution. Dotted line: Nearside angular distribution, which is sometimes indistinguishable from the PWS angular distribution on the scale of the graph. Dashed line: Farside angular distribution. The transitions shown are (a) (0,0) → (0,0), (b) (0,1) → (0,1), (c) (0,2) → (0,2), (d) (0,3) → (0,3), (e) (0,4) → (0,4), (f) (0,5) → (0,5).

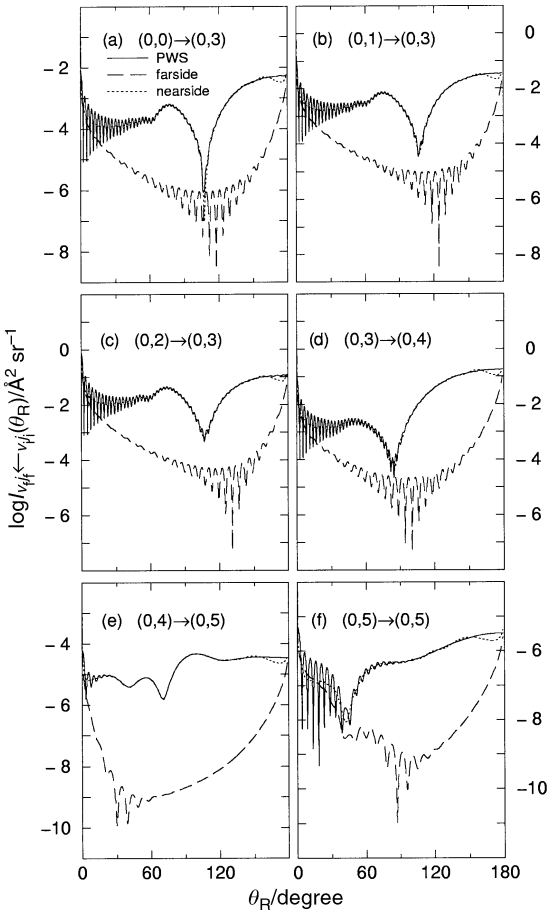

Fig. 8 Same as Fig. 7 except for $E = 26.8$ meV and the transitions (a) (0,0) → (0,3), (b) (0,1) → (0,3), (c) (0,2) → (0,3), (d) (0,3) → (0,4), (e) (0,4) → (0,5), (f) (0,5) → (0,5).

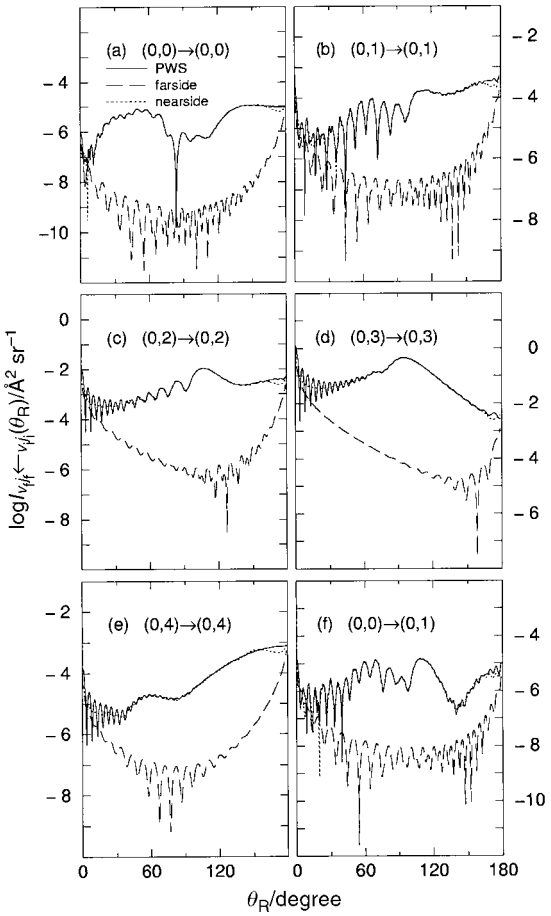

Fig. 9 Same as Fig. 7 except for $E = 21.3$ meV and the transitions (a) (0,0) → (0,0), (b) (0,1) → (0,1), (c) (0,2) → (0,2), (d) (0,3) → (0,3), (e) (0,4) → (0,4), (f) (0,0) → (0,1).

iour usually occurs where $I^{(+)}_{v_f j_f \leftarrow v_i j_i}(\theta_R) \ll I_{v_f j_f \leftarrow v_i j_i}(\theta_R)$, which does not affect the physical interpretation of the scattering.

Every N and F angular distribution diverges weakly to infinity as $\theta_R \to 0,\pi$. This unphysical behaviour arises[24] from the logarithmic singularities of $Q_J(\cos\theta_R)$ at $\theta_R = 0,\pi$.

The scattering is N dominated over most of the angular range, which is consistent with the results from the semiclassical optical model of section III. Exceptions occur for the (0,4) → (0,4) and (0,5) → (0,5) transitions at $E = 29.5$ meV in Fig. 7 (e), (f), for the (0,5) → (0,5) transition at $E = 26.8$ meV in Fig. 8(f) and for the (0,1) → (0,1) and (0,0) → (0,1) transitions at $E = 21.3$ meV in Fig. 9 (b), (f), where the N and F cross sections are of comparable magnitude for $\theta_R \lesssim 30°$.

The high frequency oscillations, which are prominent at forward angles, are clearly seen to arise from the interference of the N and F subamplitudes. A simple 'two slit' NF model gives for the oscillation period[23]

$$\Delta\theta_R = \pi/(k_{v_i j_i} r_{IH}) \qquad (4.8)$$

where r_{IH} is the I–H distance in the I–H–I complex. If we choose $r_{IH} = r^{\ddagger}_{IH} = 1.794$ Å, the approximation (4.8) gives, for $v_i = 0, j_i = 2$, periods of $\Delta\theta_R \approx 3.7°, 3.9°, 4.5°$ at $E = 29.5, 26.8, 21.3$ meV respectively, in fair agreement with the values 2.6°, 3.0°, 5.0° from Fig. 7(c), 8(c), 9(c), respectively. Evidently r_{IH} should increase with E rather than remain constant.

Fig. 7–9 show that the angular distributions also possess undulations in the range $30° \lesssim \theta_R \lesssim 120°$, which have a larger period than the high frequency NF oscillations. Moreover these undulations are clearly a N effect rather than arising from a NF interference. In ref. 14, a semiclassical Regge pole analysis was reported for the angular scattering of the (0,0) → (0,2) transition at $E = 21.3$ meV [which is similar to the (0,2) → (0,2) cross section plotted in Fig. 3(c) and 9(c)]. It was shown that the slow undulations result from the interference of a Regge pole located at ≈37.0 + 1.3i with the direct scattering for $J \lesssim 37$.

V. Conclusions

We have reported eighteen state selected differential cross sections for the isoergic I + HI reaction. We used a quantum scattering method that applied a Born–Oppenheimer type separation to the motion of the light and heavy atoms. Our results have extended earlier work by Richard-Viard *et al.*[9]

The differential cross sections displayed forward, sideward and backward scattering. Two methods were employed to analyse structure in the cross sections. The first method used a semiclassical optical method to calculate the angular distributions. It succesfully explained the backward scattering in term of simple classical concepts, but failed for the forward and sideward scattering. The second method applied an exact NF decomposition to the Legendre partial wave series for the scattering amplitude. We found that the NF method nearly always provided a clear physical interpretation of the angular scattering.

Acknowledgement

Support of this research by the Engineering and Physical Sciences Research Council (U.K.) and INTAS (E.U.) is gratefully acknowledged.

References

1 J. Manz and J. Römelt, *Chem. Phys. Lett.*, 1981, **81**, 179.
2 J. A. Kaye and A. Kuppermann, *Chem. Phys. Lett.*, 1981, **77**, 573; I. Last, *Chem. Phys.*, 1982, **69**, 193; V. Aquilanti, S. Cavalli and A. Laganà, *Chem. Phys. Lett.*, 1982, **93**, 179; C. Hiller, J. Manz, W. H. Miller and J. Römelt, *J. Chem. Phys.*, 1983, **78**, 3850; C. L.

Shoemaker, N. AbuSalbi and D. J. Kouri, *J. Phys. Chem.*, 1983, **87**, 5389; V. K. Babamov, V. Lopez and R. A. Marcus, *J. Chem. Phys.*, 1983, **78**, 5621; *erratum*, 1984, **81**, 4182; V. Aquilanti, S. Cavalli, G. Grossi and A. Laganà, *THEOCHEM*, 1984, **16**, 95; D. G. Truhlar, B. G. Garrett, P. G. Hipes and A. Kuppermann, *J. Chem. Phys.*, 1984, **81**, 3542; E. Pollak and J. Römelt, *J. Chem. Phys.*, 1984, **80**, 3613; V. Lopez, V. K. Babamov and R. A. Marcus, *J. Chem. Phys.*, 1984, **81**, 3962; M. V. Bazilevskii, V. M. Ryaboi and G. E. Chudinov, *Teoret. Éksper. Khim.*, 1985, **21**, 257 (English translation: *Theor. Exp. Chem.*, 1985, **21**, 247); J. Manz, in *Electronic Structure and Chemical Reactivity*, ed. J. Maruani, Kluwer, Dordrecht, 1989, vol. 3, pp. 365–404; R. T. Skodje and M. J. Davis, *J. Chem. Phys.*, 1988, **88**, 2429; R. T. Skodje, *J. Chem. Phys.*, 1989, **90**, 6193; M. V. Basilevsky, G. E. Chudinov and V. M. Ryaboy, *Chem. Phys.*, 1986, **104**, 265; V. K. Babamov, *Glas. Hem. Tehnol. Maked*, 1994, **13**, 13; T. C. Allison and D. G. Truhlar, in *Modern Methods for Multidimensional Dynamics Computations in Chemistry*, ed. D. L. Thompson, World Scientific, Singapore, 1998, pp. 618–712.

3 J. Römelt, *Chem. Phys.*, 1983, **79**, 197; E. Pollak, *J. Chem. Phys.*, 1983, **78**, 1228; V. Aquilanti, S. Cavalli, G. Grossi and A. Laganà, *Hyperfine Interact.*, 1984, **17–19**, 739; J. Manz, *Comments At. Mol. Phys.*, 1985, **17**, 91; J. Manz and J. Römelt, *Nachr. Chem. Tech. Lab.*, 1985, **33**, 210; J. Römelt, in *The Theory of Chemical Reaction Dynamics*, ed. D. C. Clary, Reidel, Dordrecht, 1986, pp. 77–104.

4 C. Nyeland and T. A. Bak, *Trans. Faraday Soc.*, 1965, **61**, 1293; T. Shirai, K. Iguchi and T. Watanabe, *J. Phys. Soc. Jpn.*, 1976, **40**, 1137; M. Kimura, *Chem. Phys. Lett.*, 1977, **45**, 489; D. G. Truhlar, P. C. Olsen and C. A. Parr, *J. Chem. Phys.*, 1972, **57**, 4479; B. C. Garrett and D. G. Truhlar, *J. Am. Chem. Soc.*, 1979, **101**, 4534; I. Last and M. Baer, *J. Chem. Phys.*, 1984, **80**, 3246; I. Last and Y. Shima, *Chem. Phys.*, 1986, **110**, 287; I. Last and M. Baer, *Int. J. Quant. Chem.*, 1986, **29**, 1067; I. Last and M. Baer, *J. Chem. Phys.*, 1987, **86**, 5534; H. K. Shin, *Chem. Phys. Lett.*, 1991, **179**, 483; R. T. Skodje, *J. Chem. Phys.*, 1991, **95**, 7234; B. B. Grayce and R. T. Skodje, *J. Chem. Phys.*, 1991, **95**, 7249; D. C. Chatfield, R. S. Friedman, G. C. Lynch and D. G. Truhlar, *J. Phys. Chem.*, 1992, **96**, 57; B. B. Grayce and R. T. Skodje, *J. Phys. Chem.*, 1992, **96**, 4134; R. T. Skodje, *Ann. Rev. Phys. Chem.*, 1993, **44**, 145; B. B. Grayce, R. T. Skodje and J. M. Hutson, *J. Chem. Phys.*, 1993, **98**, 3929; Z.-T. Cai, X. Zhao and C.-H. Deng, *Huaxue Xuebao* (*Acta Chim. Sin.*), 1995, **53**, 1054; D. C. Chatfield, R. S. Friedman, S. L. Mielke, G. C. Lynch, T. C. Allison and D. G. Truhlar, in *Dynamics of Molecules and Chemical Reactions*, ed. R. E. Wyatt and J. Z. H. Zhang, Marcel Dekker, New York, 1996, pp. 323–386.

5 G. C. Schatz, D. Sokolovski and J. N. L. Connor, *Faraday Discuss. Chem. Soc.*, 1991, **91**, 17.

6 C. Kubach, *Chem. Phys. Lett.*, 1989, **164**, 475.

7 C. Kubach, G. Nguyen Vien and M. Richard-Viard, *J. Chem. Phys.*, 1991, **94**, 1929.

8 G. Nguyen Vien, M. Richard-Viard and C. Kubach, *J. Phys. Chem.*, 1991, **95**, 6067.

9 M. Richard-Viard, G. Nguyen Vien and C. Kubach, *Chem. Phys. Lett.*, 1992, **188**, 525. On p. 527, 13 lines below eqn. (3), for 'smaller' read 'slower'. Four lines below eqn. (5), for '$|f_{m\rightarrow n}(\theta)|^2$' read '$(k_n/k_m)|f_{m\rightarrow n}(\theta)|^2$'.

10 G. Nguyen Vien, N. Rougeau and C. Kubach, *Chem. Phys. Lett.*, 1993, **215**, 35.

11 G. Nguyen Vien and C. Kubach, *Chem. Phys.*, 1994, **179**, 131.

12 C. Kubach and N. Rougeau, *J. Mol. Struct.* (*Theochem*), 1988, **424**, 171.

13 G. C. Schatz, *Isr. J. Chem.*, 1989, **29**, 361; G. C. Schatz, *J. Chem. Phys.*, 1989, **90**, 4847; G. C. Schatz, *J. Chem. Soc., Faraday Trans.*, 1990, **86**, 1729; G. C. Schatz, *J. Phys. Chem.*, 1990, **94**, 6157.

14 D. Vrinceanu, A. Z. Msezane, D. Bessis, J. N. L. Connor and D. Sokolovski, *Chem. Phys. Lett.*, 2000, **324**, 311.

15 D. C. Clary and J. N. L. Connor, *Chem. Phys. Lett.*, 1983, **94**, 81; D. C. Clary and J. N. L. Connor, *J. Phys. Chem.*, 1984, **88**, 2758.

16 A. Weaver, R. B. Metz, S. E. Bradforth and D. M. Neumark, *J. Phys. Chem.*, 1988, **92**, 5558; T. Kitsopoulos, R. B. Metz, A. Weaver and D. M. Neumark, in *Advances in Laser Science-III*, ed. A. C. Tam, J. L. Gole and W. C. Stwalley, American Institute of Physics, New York, 1988, pp. 573–576; S. E. Bradforth, A. Weaver, R. B. Metz and D. M. Neumark, in *Advances in Laser Science-IV*, ed. J. L. Gole, D. F. Heller, M. Lapp and W. C. Stwalley, American Institute of Physics, New York, 1989, pp. 657–663; D. M. Neumark, in *The Physics of Electronic and Atomic Collisions*, ed. A. Dalgarno, R. S. Freund, P. M. Koch, M. S. Lubell and T. B. Lucatorto, American Institute of Physics, New York, 1990, pp. 33–48; I. M. Waller, T. N. Kitsopoulos and D. M. Neumark, *J. Phys. Chem.*, 1990, **94**, 2240; D. M. Neumark, in *Advances in Molecular Vibrations and Collision Dynamics*, ed. J. M. Bowman and M. A. Ratner, JAI, Greenwich, CT, 1991, vol. 1A, pp. 165–185; R. B. Metz, S. E. Bradforth and D. M. Neumark, *Adv. Chem. Phys.*, 1992, **81**, 1; D. M. Neumark, *Annu. Rev. Phys. Chem.*, 1992, **43**, 153; R. B. Metz and D. M. Neumark, *J. Chem. Phys.*, 1992, **97**, 962; D. M. Neumark, *Acc. Chem. Res.*, 1993, **26**, 33; Z. Liu, H. Gómez and D. M. Neumark, *Chem. Phys. Lett.*, 2000, **332**, 65; Z. Liu, H. Gómez and D. M. Neumark, *Faraday Discuss.*, 2001, **118**, 221.

17 B. Gazdy and J. M. Bowman, *J. Chem. Phys.*, 1989, **91**, 4615; J. M. Bowman and B. Gazdy, *J. Phys. Chem.*, 1989, **93**, 5129; V. Engel, *J. Chem. Phys.*, 1991, **94**, 16; G. C. Schatz, S. Florance, T. J. Lee and C. W. Bauschlicher, Jr., *Chem. Phys. Lett.*, 1993, **202**, 495.

18 G. C. Schatz, D. Sokolovski and J. N. L. Connor, *J. Chem. Phys.*, 1991, **94**, 4311; W. Jakubetz, D. Sokolovski, J. N. L. Connor and G. C. Schatz, *J. Chem. Phys.*, 1992, **97**, 6451; G. C. Schatz, D. Sokolovski and J. N. L. Connor, in *Advances in Molecular Vibrations and Collision Dynamics*, ed. J. M. Bowman, JAI, Greenwich, CT, 1994, vol. 2B, pp. 1–26; R. T. Skodje, D. Skouteris, D. E. Manolopoulos, S.-H. Lee, F. Dong and K. Liu, *J. Chem. Phys.*, 2000, **112**, 4536; K. Liu, *Nucl. Phys. A*, 2001, **684**, 247c.

19 J. Manz, R. Meyer, E. Pollak and J. Römelt, *Chem. Phys. Lett.*, 1982, **93**, 184; E. Pollak, in *Intramolecular Dynamics*, ed. J. Jortner and B. Pullman, Reidel, Dordrecht, 1982, pp. 1–16; E. Pollak, *Chem. Phys. Lett.*, 1983, **94**, 85; J. Manz, R. Meyer and J. Römelt, *Chem. Phys. Lett.*, 1983, **96**, 607; E. Pollak, *Comments At. Mol. Phys.*, 1984, **15**, 73; J. Manz, R. Meyer, E. Pollak, J. Römelt and H. H. R. Schor, *Chem. Phys.*, 1984, **83**, 333; J. Manz, R. Meyer and H. H. R. Schor, *J. Chem. Phys.*, 1984, **80**, 1562; J. Römelt and E. Pollak, in *Resonances in Electron—Molecule Scattering, van der Waals Complexes and Reactive Chemical Dynamics*, ed. D. G. Truhlar, American Chemical Society, Washington, DC, 1984, pp. 353–374; R. Lefebvre, *Ann. Phys.*, 1990, **15**, 1.

20 D. R. Herschbach, *Appl. Opt.*, 1965, Suppl. No. 2, 128; D. R. Herschbach, *Adv. Chem. Phys.*, 1966, **10**, 319.

21 J. N. L. Connor, P. McCabe, D. Sokolovski and G. C. Schatz, *Chem. Phys. Lett.*, 1993, **206**, 119.

22 D. Sokolovski, J. N. L. Connor and G. C. Schatz, *Chem. Phys. Lett.*, 1995, **238**, 127.

23 D. Sokolovski, J. N. L. Connor and G. C. Schatz, *J. Chem. Phys.*, 1995, **103**, 5979.

24 P. McCabe and J. N. L. Connor, *J. Chem. Phys.*, 1996, **104**, 2297.

25 D. Sokolovski, J. N. L. Connor and G. C. Schatz, *Chem. Phys.*, 1996, **207**, 461.

26 J. Wimp, P. McCabe and J. N. L. Connor, *J. Comput. Appl. Math.*, 1997, **82**, 447.

27 P. McCabe, J. N. L. Connor and D. Sokolovski, *J. Chem. Phys.*, 1998, **108**, 5695.

28 D. Sokolovski and J. N. L. Connor, *Chem. Phys. Lett.*, 1999, **305**, 238.

29 J. J. Hollifield and J. N. L. Connor, *Phys. Rev. A*, 1999, **59**, 1694.

30 J. J. Hollifield and J. N. L. Connor, *Mol. Phys.*, 1999, **97**, 293.

31 A. J. Dobbyn, P. McCabe, J. N. L. Connor and J. F. Castillo, *Phys. Chem. Chem. Phys.*, 1999, **1**, 1115.

32 P. McCabe, J. N. L. Connor and D. Sokolovski, *J. Chem. Phys.*, 2001, **114**, 5194.

33 T. W. J. Whiteley, C. Noli and J. N. L. Connor, *J. Phys. Chem. A*, 2001, **105**, 2792.

34 B. C. Garrett, D. G. Truhlar, A. F. Wagner and T. H. Dunning, Jr., *J. Chem. Phys.*, 1983, **78**, 4400; M. A. Vincent, J. N. L. Connor, M. S. Gordon and G. C. Schatz, *Chem. Phys. Lett.*, 1993, **203**, 415; C. S. Maierle, G. C. Schatz, M. S. Gordon, P. McCabe and J. N. L. Connor, *J. Chem. Soc., Faraday Trans.*, 1997, **93**, 709; M. González, J. Hijazo, J. J. Novoa and R. Sayós, *J. Chem. Phys.*, 1998, **108**, 3168; A. J. Dobbyn, J. N. L. Connor, N. A. Besley, P. J. Knowles and G. C. Schatz, *Phys. Chem. Chem. Phys.*, 1999, **1**, 957; J. Espinosa-García, *J. Phys. Chem. A*, 2001, **105**, 134.

35 G. C. Schatz, B. Amaee and J. N. L. Connor, *J. Phys. Chem.*, 1988, **92**, 3190.

36 N. Rougeau and C. Kubach, *Chem. Phys.*, 1993, **175**, 299; N. Rougeau and C. Kubach, *Chem. Phys. Lett.*, 1994, **228**, 207; N. Rougeau and C. Kubach, *J. Mol. Struct.* (*Theochem.*), 1995, **330**, 57; N. Rougeau and C. Kubach, *Chem. Phys. Lett.*, 1995, **246**, 664; N. Rougeau, S. Marcotte and C. Kubach, *J. Chem. Phys.*, 1996, **105**, 8653; N. Rougeau and C. Kubach, *Chem. Phys. Lett.*,

1997, **274**, 535; N. Rougeau and C. Kubach, *Chem. Phys. Lett.*, 1999, **299**, 120; N. Rougeau, G. Nyman and C. Kubach, *Phys. Chem. Chem. Phys.*, 1999, **1**, 1191; N. Rougeau and C. Kubach, *Phys. Chem. Chem. Phys.*, 2000, **2**, 701.

37 M. A. Collins and R. G. Gilbert, *Chem. Phys. Lett.*, 1976, **41**, 108; J. L. Kinsey, G. H. Kwei and D. R. Herschbach, *J. Chem. Phys.*, 1976, **64**, 1914; M. L. Vestal, A. L. Wahrhaftig and J. H. Futrell, *J. Phys. Chem.*, 1976, **80**, 2892; S. M. McPhail and R. G. Gilbert, *Chem. Phys.*, 1978, **34**, 319; G. H. Kwei and D. R. Herschbach, *J. Phys. Chem.*, 1979, **83**, 1550; N. Agmon, *Chem. Phys.*, 1981, **61**, 189; R. E. Wyatt, J. F. McNutt and M. J. Redmon, *Ber. Bunsen-Ges. Phys. Chem.*, 1982, **86**, 437; N. Agmon, *Int. J. Chem. Kinet.*, 1986, **18**, 1047; G. C. Schatz, B. Amaee and J. N. L. Connor, *Comput. Phys. Commun.*, 1987, **47**, 45; G. C. Schatz, B. Amaee and J. N. L. Connor, *J. Chem. Phys.*, 1990, **93**, 5544.

38 K. Takayanagi, *Prog. Theor. Phys.*, 1952, **8**, 497; J. M. Bowman, *Adv. Chem. Phys.*, 1985, **61**, 115; Q. Sun, J. M. Bowman, G. C. Schatz, J. R. Sharp and J. N. L. Connor, *J. Chem. Phys.*, 1990, **92**, 1677; J. M. Bowman, *J. Phys. Chem.*, 1991, **95**, 4960.

39 R. C. Fuller, *Phys. Rev. C*, 1975, **12**, 1561.